Biol Cybern (2011) 105:167–180
DOI 10.1007/s00422-011-0458-2

ORIGINAL PAPER

Biological Cybernetics

Comparison of different neuron models to conductance-based post-stimulus time histograms obtained in cortical pyramidal cells using dynamic-clamp in vitro

Martin Pospischil · Zuzanna Piwkowska · Thierry Bal · Alain Destexhe

Received: 24 October 2010 / Accepted: 7 September 2011 / Published online: 5 October 2011
© Springer-Verlag 2011

Abstract A wide diversity of models have been proposed to account for the spiking response of central neurons, from the integrate-and-fire (IF) model and its quadratic and exponential variants, to multiple-variable models such as the Izhikevich (IZ) model and the well-known Hodgkin–Huxley (HH) type models. Such models can capture different aspects of the spiking response of neurons, but there is few objective comparison of their performance. In this article, we provide such a comparison in the context of well-defined stimulation protocols, including, for each cell, DC stimulation, and a series of excitatory conductance injections, arising in the presence of synaptic background activity. We use the dynamic-clamp technique to characterize the response of regular-spiking neurons from guinea-pig visual cortex by computing families of post-stimulus time histograms (PSTH), for different stimulus intensities, and for two different background activities (low- and high-conductance states). The data obtained are then used to fit different classes of models such as the IF, IZ, or HH types, which are constrained by the whole data set. This analysis shows that HH models are generally more accurate to fit the series of experimental PSTH, but their performance is almost equaled by much simpler models, such as the exponential or pulse-based IF models. Similar conclusions were also reached by performing partial fitting of the data, and examining the ability of different models to predict responses that were not used for the fitting. Although such results must be qualified by using more sophisticated stimulation protocols, they suggest that nonlinear IF models can capture surprisingly well the response of cortical regular-spiking neurons and appear as useful candidates for network simulations with conductance-based synaptic interactions.

M. Pospischil · Z. Piwkowska · T. Bal · A. Destexhe (✉)
Unité de Neurosciences, Information et Complexité (UNIC), CNRS, Gif-sur-Yvette, France
e-mail: destexhe@unic.cnrs-gif.fr

Keywords Spiking neuron models · Model fitting · Genetic algorithms · In vitro · Cerebral cortex

1 Introduction

Since the early days of computational neuroscience, a plurality of different neuron models have been proposed, among which the leaky integrate-and-fire (leaky IF, Lapicque 1907) and the Hodgkin–Huxley (HH, Hodgkin and Huxley 1952) models are probably the best known and most used ones. They also constitute a sort of frame, with on the one hand the leaky IF model rather being a sketch of a spiking model, compared to the detailed analogy between state variables in the HH model and ion channels in biological neurons on the other hand. A multitude of models have been developed over the years that fall within this frame. The extension of the leaky IF model has lead to a whole family of nonlinear IF models (e.g., the quadratic or the exponential IF models, Ermentrout 1996; Latham et al. 2000; Fourcaud-Trocmé et al. 2003), whereas the reduction of the HH model gave rise to a different type of models, where spikes result from the interplay of two coupled state variables (e.g., the Fitzhugh–Nagumo or the Morris–Lecar models, Fitzhugh 1961; Nagumo et al. 1962; Morris and Lecar 1981). Another approach was to obtain an analytically solvable HH model by replacing the complex voltage- and time-dependence of the rate constants by a pulse triggered when the V_m crosses a given threshold (Destexhe, 1997). These "pulse-based" IF models capture the Na^+ and K^+ conductance interplay during and after action potentials, and naturally handle the spike shape, the refractory period and the resetting of the V_m. Some of these IF models were recently unified by Izhikevich (2003), and later extended to the adaptive exponential IF model (Brette and Gerstner 2005). In these models, subthreshold dynamics are

described by two coupled state variables, but spiking is still realized in terms of thresholds and reset values.

Clearly, the models differ in their capability to qualitatively reproduce firing types seen in cortical neurons, and usually (though not always) the more elaborate models cover a broader range (see Izhikevich 2004 for a summary). A different question, however, is the following: for a given neuron, how well do the models reproduce a particular firing pattern quantitatively? Different approaches have been followed in order to address this question. Some consist in assuming that a given detailed model represents a good candidate for biological behavior, which then serves as a benchmark in the attempt to match one or several simpler models to it (cf., e.g., Fourcaud-Trocmé et al. 2003; Jolivet et al. 2004; Brette and Gerstner 2005). Another approach consists in directly matching models to data obtained in experiments (e.g., Jolivet et al. 2006; Jolivet et al. 2008; Clopath et al. 2007; Pospischil et al. 2008; Goaillard et al. 2009). Sometimes, one and the same model is matched to itself for the purpose of exploring the underlying "parameter landscape" (Achard and De Schutter 2006) or comparing the capacity of different optimization techniques (Weaver and Wearne 2006). The protocols used in these cases are diverse. They comprise both current and conductance injections, where the waveforms range from simple square pulses to stochastically fluctuating traces.

The matching itself can also be accomplished along various lines. Besides the widely used, straight forward "hand tuning", less biased techniques have been employed. In some cases it is possible to determine model parameters from standard electrophysiological protocols. For example, it is conventional to extract input resistance and capacitance of a neuron from current pulse injections. But while for some models it is possible to obtain all parameter values in such a direct way, for others it is not and automated optimization techniques have to be applied. Comparative studies of such techniques have been reviewed previously (Vanier and Bower 1999; Van Geit et al. 2008). For the problem treated therein, the simulated annealing algorithm is clearly favored. However, the performance of an optimization technique also depends on the objective function. While for a fit of subthreshold properties it might be sufficient to base the objective function on the time course of the membrane potential, in general this is not a good choice for spiking neurons. Here, shifts in spike times of the order of the spike width will introduce large jumps in the assigned error. A different approach has been taken in Vanier and Bower (1999), where the objective function is basically composed as a sum over differences in spike time between model and target, normalized by the time of the respective spike in the model. In the cases where a neuron model constitutes its own target, it is possible to use more sophisticated objective functions by either taking into account the spike shape (Weaver and Wearne 2006), or by using the neuron's probability density in the (V_m − dV_m/dt)—plane (Achard and De Schutter 2006; Le Masson and Maex 2001). It is not clear, however, how the latter performs when model and data are based on different dynamical systems.

In this article, we compare the capacity of eight different neuron models, spanning the complexity spectrum between the leaky IF and the HH model, to quantitatively reproduce the behavior of four different cortical neurons, that were recorded in vitro using dynamic clamp. Since the neurons are regular spiking (RS), we include an adaptation mechanism in all models. The protocols used are intended to classify adaptation (using DC stimulation) or to recreate conditions that are close to natural network states. During the latter, the neuron (and the models) are injected with two channels of fluctuating conductances (point-conductance model, Destexhe et al. 2001) intended to represent the input of excitatory and inhibitory presynaptic neurons, respectively. We contrast two different background states: the first is a "low conductance" (LC) state, where the mean values of excitatory and inhibitory conductances are approximately equal and comparable in magnitude to the leak conductance. The other is a "high conductance" (HC) state, characterized by dominant inhibition and a leak conductance that is small compared to the synaptic conductances. For each conductance state, a whole family of AMPA-shaped stimuli are injected, thus forming a very constraining data set to be reproduced by models. The post-stimulus time histograms (PSTHs) of the models are then compared to the ones of the target cells, in the same conditions. We fit the models either to one background state at a time and predict the PSTH for the respective other state, or we fit the PSTHs obtained in both states simultaneously.

2 Materials and methods

2.1 In vitro experiments

In vitro experiments were performed on 380–400 μm thick coronal slices from the lateral portions of guinea-pig occipital cortex. Guinea-pigs, 4–12 weeks old (CPA, Olivet, France), were anesthetized with sodium pentobarbital (30 mg/kg). The slices were maintained in an interface style recording chamber at 33–35°C. Slices were prepared on a DSK micro-slicer (Ted Pella Inc., Redding, CA) in a slice solution in which the NaCl was replaced with sucrose while maintaining an osmolarity of 307 mOsm. During recording, the slices were incubated in slice solution containing (in mM): NaCl, 124; KCl, 2.5; $MgSO_4$, 1.2; $NaHPO_4$, 1.25; $CaCl_2$, 2; $NaHCO_3$, 26; dextrose, 10, and aerated with 95% O_2, 5% CO_2 to a final pH of 7.4. Intracellular recordings following two hours of recovery were performed in all cortical layers in electrophysiologically identified regular spiking cells. Electrodes for intracellular recordings were made on a Sutter Instru-

ments P-87 micropipette puller from medium-walled glass (WPI, 1BF100) and beveled on a Sutter Instruments beveler (BV-10M). Micropipettes were filled with 1.2–2 M potassium acetate—4 mM potassium chloride and had resistances of 65–110 MΩ after beveling.

The dynamic-clamp technique (Robinson and Kawai 1993; Sharp et al. 1993) was used to inject computer-generated conductances in real neurons. Dynamic-clamp experiments were run using the hybrid RT-NEURON environment (Le Franc et al. 2001; Sadoc et al. 2009), which is a modified version of NEURON (Hines and Carnevale 1997) running under the Windows operating system (Microsoft Corp.). NEURON was augmented with the capacity of simulating neuronal models in real time, synchronized with the intracellular recording. To achieve real-time simulations as well as data transfer to the PC for further analysis, we used a PCI DSP board (Innovative Integration, Simi Valley, USA) with 4 analog/digital (inputs) and 4 digital/analog (outputs) 16 bits converters. The DSP board allows input (for instance the membrane potential of the real cell incorporated in the equations of the models) and output signals (the synaptic current to be injected into the cell) to be processed at regular intervals (time resolution = 0.1 ms). A custom interface was used to connect the digital and analog inputs/outputs signals of the DSP board with the intracellular amplifier (Axoclamp 2B, Axon Instruments) and the data acquisition systems (PC-based acquisition software ELPHY, developed by G. Sadoc, CNRS Gif-sur-Yvette, ANVAR and Biologic). The dynamic-clamp protocol was used to insert the fluctuating conductances underlying synaptic noise in cortical neurons using the point-conductance model, similar to previous studies (Destexhe et al. 2001; Piwkowska et al. 2008). The injected current is determined from the fluctuating conductances $g_e(t)$ and $g_i(t)$ as well as from the difference between the recorded membrane voltage V and the respective reversal potentials, $I_{\mathrm{DynClamp}} = -g_e\big(V - V_e\big) - g_i\big(V - V_i\big)$. The contamination of the recorded membrane voltage by electrode artefacts was avoided through the use of active electrode compensation, a novel, high-resolution digital on-line compensation technique that we have recently developed (Brette et al. 2008).

All research procedures concerning the experimental animals and their care adhered to the American Physiological Society's Guiding Principles in the Care and Use of Animals, to the European Council Directive 86/609/EEC and to European Treaties series no. 123, and were also approved by the local ethics committee "Ile-de-France Sud" (certificate no. 05-003).

2.2 Models

For the simulations, we use single compartment models of varying complexity in an attempt to reproduce the adapting spike trains and the PSTHs obtained during experiments. The details of the mechanism that accounts for spike rate adaptation depends on the type of model. We assume that the capacitance of the cell as well as its leak conductance and leak reversal potential can be deduced from the experiment, hence these parameters are kept fixed during the optimization. All other parameters are allowed to vary freely, except for the HH model, where only a subset of parameters was adjusted. In the following, we describe the models in ascending order of complexity.

2.3 Integrate-and-fire models

We use four different integrate-and-fire (IF) models, that are distinguished by their I–V relation. First, we use the linear or leaky IF model (Lapicque 1907). It is described by the membrane equation

$$C\frac{\mathrm{d}V}{\mathrm{d}t} = -g_L(V - V_L) - g_K(V - V_K) + I_{\mathrm{ext}}, \tag{1}$$

which in addition to the classic definition contains a conductance g_K, that accounts for spike rate adaptation (see Eq. 5 below). Further parameters are the leak conductance and reversal potential g_L and V_L as well as the capacitance C. The model can be driven by an additional input current I_{ext}. It is said to fire a spike whenever the voltage V reaches a fixed threshold V_{th}, after which the integration restarts at the reset potential V_R. Modifications to this model have been suggested, in order to obtain biophysically more plausible behavior. The most prominent among these so called nonlinear IF models are probably the quadratic (Ermentrout 1996; Latham et al. 2000) as well as the exponential IF model (Fourcaud-Trocmé et al. 2003). We slightly vary the definition given in Fourcaud-Trocmé et al. (2003):

$$C\frac{\mathrm{d}V}{\mathrm{d}t} = -g_{\mathrm{L}}(V - V_{\mathrm{L}}) + \psi(V) - g_K(V - V_K) + I_{\mathrm{ext}}. \tag{2}$$

The nonlinearity $\psi(V)$ is given by

$$\psi(V) = \begin{cases} \frac{g_{\mathrm{L}}}{2\Delta_{\mathrm{T}}}(V - V_{\mathrm{T}})^2 & \text{quadratic IF (qIF) model} \\ \quad +g_{\mathrm{L}}(V - V_{\mathrm{L}}) - I_{\mathrm{T}} & \\ g_{\mathrm{L}}\,\Delta_{\mathrm{T}}\,\exp\left(\frac{V - V_{\mathrm{T}}}{\Delta_{\mathrm{T}}}\right) & \text{exponential IF (eIF) model} \end{cases} \tag{3}$$

In both cases, a spike is said to be fired when the membrane potential diverges to infinity (in practice, the time of the spike is calculated when the membrane potential is sufficiently depolarized, such as 0 mV). V is subsequently set to the reset potential V_{R}. There are three additional parameters: V_{T} is the threshold voltage, i.e., the largest voltage at which the neuron can be maintained during constant current injection without firing a spike. Δ_{T} is the spike slope factor, which controls the rapidity of spike initiation; for $\Delta_{\mathrm{T}} \to 0$ the exponential IF model degenerates to its linear analog. For

the quadratic IF model I_T is the threshold current, i.e., a constant injected current of amplitude I_T depolarizes the neuron voltage to V_T.

We also used a hybrid IF model that is identical to the linear IF model for voltages below a fixed value V_C, and whose I–V curve rises quadratically whenever the voltage exceeds V_C. This model was called the "linear-quadratic IF" (lqIF) model in the following and is described by Eq. 2, where

$$\psi(V) = \begin{cases} 0 & V < V_C \\ \frac{g_L}{2\Delta_T}(V - V_T)^2 + g_L(V - V_L) - I_T & V \geq V_C \end{cases} \quad (4)$$

V_C as well as I_T are determined from the condition that $\psi(V)$ as well as its first derivative be continuous for $V \to V_C$. They are given by $V_C = V_T - \Delta_T$ and $I_T = -g_L\left(\frac{\Delta_T}{2} + V_L - V_T\right)$. Spiking is realized in the same way as for the other nonlinear IF models.

All these models use the same mechanism for spike rate adaptation, a potassium channel with conductance g_K that reverses at the potential $V_K = -90\,\mathrm{mV}$. A state variable m is augmented by a quantum $q = 1$ following each spike and subsequently decays exponentially with time constant τ_K,

$$\frac{\mathrm{d}m}{\mathrm{d}t} = -\frac{m}{\tau_K}. \quad (5)$$

The conductance is then given by the product $g_K = \bar{g}_K m$. Both parameters, $\bar{g}_K$ and τ_K are adjusted during the optimization.

2.4 The 2-state-variable models

We use two models of intermediate complexity, the Izhikevich model (Izhikevich 2003) as well as the adaptive exponential IF (aEIF) model (Brette and Gerstner 2005). In addition to the membrane potential, both models comprise a second state variable that is responsible for subthreshold and supra-threshold adaptation. The defining equations of the Izhikevich model are

$$C\frac{\mathrm{d}V}{\mathrm{d}t} = k(V - V_L)(V - V_T) - w + I_{\mathrm{ext}}, \quad (6)$$

$$\frac{\mathrm{d}w}{\mathrm{d}t} = a(b(V - V_L) - w). \quad (7)$$

A spike is released when the voltage exceeds 30 mV, after which it is reset to V_R and a fixed value d is added to the adaptation variable ($w \to w + d$). The aEIF model is defined in a similar way, except that the subthreshold I–V-relation contains an exponential nonlinearity rather than a quadratic one:

$$C\frac{\mathrm{d}V}{\mathrm{d}t} = -g_L(V - V_L) + g_L\Delta_T \exp\left(\frac{V - V_T}{\Delta_T}\right) - w + I_{\mathrm{ext}} \quad (8)$$

$$\tau_w\frac{\mathrm{d}w}{\mathrm{d}t} = a(V - V_L) - w. \quad (9)$$

If $V_m > 20\,\mathrm{mV}$ a spike is released, after which the voltage is reset to V_R and the adaptation variable augmented by b ($w \to w + b$). During the simulations where no adaptation current was included, in both models we skipped the update of the adaptation variable following a spike, i.e., we set $d = 0$ in the Izhikevich model and $b = 0$ in the aEIF model. Again, we assumed that the capacitance C as well as the leak conductance and reversal potential g_L and V_L are extracted from the experiment, all other parameters being adjusted during the fit in order to obtain optimal behavior. However, while the parameters C and V_L in the models directly represent the respective physiological quantities, this is not the case for the leak conductance: after replacing w in Eqs. 6 and 8 by its equilibrium value (obtained from the condition $\mathrm{d}w/\mathrm{d}t = 0$) and rewriting them as $C\,\mathrm{d}V/\mathrm{d}t = -f(V) + I_{\mathrm{ext}}$, the physiological leak conductance is given by

$$g_L^{\mathrm{physiol}} = \left.\frac{\mathrm{d}f(V)}{\mathrm{d}V}\right|_{V=V_L}. \quad (10)$$

Thus, for the Izhikevich model we obtain the relation $g_L^{\mathrm{physiol}} = b - k(V_L - V_T)$, for the aEIF model it reads $g_L^{\mathrm{physiol}} = g_L\left(1 - \exp\left(\frac{V_L - V_T}{\Delta_T}\right)\right) + a$. For typical parameter values the exponential term can be neglected, so during the simulations we used $g_L^{\mathrm{physiol}} = g_L + a$.

2.5 The Hodgkin–Huxley model

Finally, we use a Hodgkin–Huxley (HH) model comprising two channels, a fast sodium channel (g_{Na}) and a delayed rectifier potassium channel (g_{Kd}, details can be found in Traub and Miles (1991)), specified by the following membrane equation:

$$C\frac{\mathrm{d}V}{\mathrm{d}t} = -g_L(V - V_L) - g_{\mathrm{Na}}(V - V_{\mathrm{Na}}) - g_{\mathrm{Kd}}(V - V_K) - g_M(V - V_K) + I_{\mathrm{ext}}. \quad (11)$$

Also, a muscarinic conductance (g_M) accounting for adaptation has been included. The conductances g_{Na} and g_{Kd} are governed by the three state variables m, h, and n and respective maximal conductances $\bar{g}_{\mathrm{Na}}$, $\bar{g}_{\mathrm{Kd}}$:

$$g_{\mathrm{Na}} = \bar{g}_{\mathrm{Na}} m^3 h, \quad (12)$$

$$g_{\mathrm{Kd}} = \bar{g}_{\mathrm{Kd}} n^4. \quad (13)$$

The state variables evolve according to the time evolution equations

$$\frac{\mathrm{d}s}{\mathrm{d}t} = \frac{s_\infty(V) - s(t)}{\tau_s(V)}, \qquad s = \{m, h, n\}, \quad (14)$$

where the functions $s_\infty(V)$ and $\tau_s(V)$ are composed of the respective forward- and backward-rates between open and closed states, α_s and β_s:

$$s_\infty(V) = \frac{\alpha_s(V)}{\alpha_s(V) + \beta_s(V)} \tag{15}$$

$$\tau_s(V) = \frac{1}{\alpha_s(V) + \beta_s(V)}. \tag{16}$$

For the state variable m, α, and β are parameterized as

$$\alpha_m(V) = -\frac{f_a(V - V_{0,a})}{\exp\left(-\frac{V-V_{0,a}}{d_a}\right) - 1} \tag{17}$$

$$\beta_m(V) = \frac{f_b(V - V_{0,b})}{\exp\left(\frac{V-V_{0,b}}{d_b}\right) - 1}. \tag{18}$$

The muscarinic conductance g_M is described by similar equations, details can be found in Yamada et al. (1989). During optimization of the DC response, we vary the maximal conductances of the spike initiating channels, $\bar{g}_{Na}$ and $\bar{g}_{Kd}$, as well as three parameters shifting the activation and inactivation curves of sodium and potassium. In addition, we vary the maximal conductance of the adaptation channel and a parameter scaling its time constant. When optimizing the PSTH response, we vary all parameters describing the sodium activation curve, i.e., f_a, $V_{0,a}$, d_a, f_b, $V_{0,b}$, and d_b, as well as a parameter introducing a relative voltage shift between sodium activation and inactivation. The shape of the latter as well as the potassium activation curve are kept fixed. In addition, as before, we adjust the maximal conductances of the spike-related sodium and potassium channels, $\bar{g}_{Na}$ and $\bar{g}_{Kd}$, and that of the muscarinic current, $\bar{g}_M$ as well as a parameter scaling its time constant.

2.6 The pulse-based model

A simplification of the HH model has been proposed (Destexhe 1997), that aims in a different direction than has been mentioned before. It approximates the forward- and backward-rates of the three state variables m, h, and n by pulses that are triggered whenever the membrane potential crosses a threshold value V_{th}. This approximation is based on the observation that during a spike, the time course of the rates is close to a square wave. Approximating them by piecewise constant functions (pulses), it is then possible to give analytic expressions for the time course of m, h, and n before, during and after the spike. This leads to an IF model with realistic spike shape and membrane conductance changes (Destexhe 1997).

The values of the pulse functions were given by:

$$\begin{aligned} \alpha_m &= 0, & \beta_m &= \beta_M \\ \alpha_h &= \alpha_H & \beta_h &= 0 \\ \alpha_n &= 0, & \beta_n &= \beta_N \end{aligned}$$

between pulses and

$$\begin{aligned} \alpha_m &= \alpha_M, & \beta_m &= 0 \\ \alpha_h &= 0, & \beta_h &= \beta_H \\ \alpha_n &= \alpha_N, & \beta_n &= 0 \end{aligned}$$

during the pulse. The time course of the state variables is then given by

$$\begin{aligned} m(t) &= m_0 \exp[-\beta_M (t - t_0)] \\ h(t) &= 1 + (h_0 - 1) \exp[-\alpha_H (t - t_0)] \\ n(t) &= n_0 \exp[-\beta_N (t - t_0)] \end{aligned}$$

in between pulses and

$$\begin{aligned} m(t) &= 1 + (m_0 - 1) \exp[-\alpha_M (t - t_0)] \\ h(t) &= h_0 \exp[-\beta_H (t - t_0)] \\ n(t) &= 1 + (n_0 - 1) \exp[-\alpha_N (t - t_0)] \end{aligned}$$

during the pulse. We use the values

$$\begin{aligned} \alpha_M &= 22\ \text{ms}^{-1}, & \beta_M &= 13\ \text{ms}^{-1}, \\ \alpha_H &= 0.5\ \text{ms}^{-1}, & \beta_H &= 4\ \text{ms}^{-1}, \\ \alpha_N &= 2.2\ \text{ms}^{-1}, & \beta_N &= 0.76\ \text{ms}^{-1}. \end{aligned}$$

These values were optimized to fit a Hodgkin–Huxley model for action potentials in central neurons (Destexhe 1997). These values were kept fixed in this study. The adaptation mechanism, when needed, was the same as for the HH model (Yamada et al. 1989).

2.7 The protocol

We applied the same two stimulation protocols to cortical neurons in vitro and to the models described above.

The first stimulation protocol simply consisted in the stimulation of the cells with two different constant currents, upon which the cells started emitting action potentials with increasing interspike intervals (ISIs). The current amplitude depended on the cell, the pulse duration was 2 s.

The second protocol (cf. Fig. 2) consisted in a background stimulation provided by the "point-conductance model" (Destexhe et al. 2001), which simulates background synaptic conductances. This model creates two channels of fluctuating conductances, one excitatory ($g_e(t)$) and one inhibitory ($g_i(t)$), each described by Ornstein–Uhlenbeck equations. For the excitatory channel, the time evolution equation reads

$$\frac{dg_e(t)}{dt} = -\frac{1}{\tau_e}\left(g_e(t) - g_{e0}\right) + \sqrt{\frac{2\sigma_e^2}{\tau_e}}\xi_e(t). \tag{19}$$

We use g_{e0} and σ_e to indicate the mean and standard deviation (SD) of the excitatory conductance distribution, $\xi_e(t)$ is a Gaussian white noise process with zero mean and unit standard deviation and τ_e is the excitatory correlation time

constant. The inhibitory channel is described by an equivalent equation with parameters g_{i0}, σ_i, $\xi_i(t)$, and τ_i. Throughout this article we use the correlation times $\tau_e = 2.728$ and $\tau_i = 10.49$ ms. In particular, we consider two possible background states: a "low-conductance (LC) state", where excitatory and inhibitory conductances have roughly the same mean value and their sum is smaller or of the same order as the leak conductance, and a "high-conductance (HC) state", which is characterized by a dominant inhibitory conductance and a leak conductance that constitutes only a fraction of the total conductance. In addition to the background conductance, an AMPA-stimulus (see Destexhe et al. 1994 for details) of varying strength is injected in intervals of 100 ms. Its strength can take one of the five values 1 nS and 1–4 times a base strength $\bar{g}_S$, whose value depends on the cell under consideration. Subsequently, the stimulus-triggered spiking response (post-stimulus time histogram, PSTH) is calculated with a bin width of 1 ms for each stimulus strength separately. The recording time during the experiments was about 300 s for each background state (corresponding to about 600 repetitions per stimulus strength), in the models the simulated time was 100 s per background state and stimulus strength (1000 repetitions per stimulus strength).

2.8 The optimization

The optimization was done using a NEURON (Hines and Carnevale 1997) implementation of the simulated annealing method based on a simplex algorithm (Press et al. 1992). The strategy consists of a simplex (an assembly of n points, where n is the number of parameters) that moves in parameter space, where uphill steps are accepted with a certain probability depending on a slowly decreasing variable E (the 'temperature'). For very low temperature, the method becomes identical to the simplex algorithm, but during optimization it is less likely to be caught in local minima. A comparative survey (Vanier and Bower 1999) showed that for an intermediate number of parameters, the simulated annealing procedure was superior to other methods.

The error functions for both protocols consisted of both a common as well as an individual part. While the individual part took care of the actual respective signal, the common part was introduced to control the mean voltage level during stimulation. The error value to be minimized was then composed of these two parts using a weighted sum:

$$e = \frac{w_1 e^{\text{ind}} + w_2 e^{\text{com}}}{w_1 + w_2}, \tag{20}$$

with $w_1 = 4$ and $w_2 = 1$ the respective weights. The common part was defined as

$$e^{\text{com}} = \frac{|\bar{V}^{\text{sim}} - \bar{V}^{\text{data}}|}{10\,\text{mV}}, \tag{21}$$

such that a deviation in the mean voltage between model and data of 10 mV corresponds to an error of one.

The error function for fitting the DC response is given by the RMS (root mean square) of five observables: the time of the first spike after stimulus onset as well as the duration of the first, second, third, and last ISI. Before summation, each observable is normalized by its experimental value. Also, the contribution of the last interval is multiplied by four in order to equalize the relative importance of the initial and the final phase of the response:

$$e^{\text{ind}} = \sum_i f_i \frac{\sqrt{(x_i^{\text{data}} - x_i^{\text{sim}})^2}}{x_i^{\text{data}}} \Bigg/ \sum_i f_i, \tag{22}$$

where x_i stands for the observables, $f_i = 4$ for x_i representing the last ISI and $f_i = 1$ otherwise. Using this normalization, the error assigned to the case where all observables are zero is one, independent of the cell under consideration.

For the fitting of the PSTH, the error function consisted of the RMS of the difference between the experimental and the simulated PSTHs in the first 20 ms taken across all background states and stimulus strength under consideration, normalized by the RMS of the experimental PSTH:

$$e^{\text{ind}} = \sqrt{\frac{\sum_{b,s,i} (\text{psth}_i^{\text{exp}} - \text{psth}_i^{\text{sim}})^2}{\sum_{b,s,i} (\text{psth}_i^{\text{exp}})^2}}, \tag{23}$$

with the subscript b indicating the background state, s the stimulus strength and i the bin number. With this definition, an error of 1 corresponds to the complete absence of a response to the stimulus.

Simulations were performed on Linux PCs using the NEURON simulation environment (Hines and Carnevale 1997) (for the HH model) or custom C^{++} programs (for the other models).

3 Results

Recordings were taken from four different cells. It is important to note that recordings were made from a much larger database, but the full set of stimulation protocols, including the time necessary for adjusting the parameters of the injected conductances in each cell, required to keep stable recordings for a long time (1–2 h). Cells that were not strictly stable, either through V_m drifts, or changes in input resistance, were discarded. Recordings which were lost before the end of the stimulation protocol were also discarded. We obtained four cells satisfying the criteria of stability and completion of the full protocol. Their passive properties as well as stimulation details are summarized in Table 1, the voltage time course resulting from DC injection is shown in Fig. 1. The conductance parameters for the LC state were chosen such that

Table 1 Cell parameters

Cell	C (nF)	g_L (nS)	V_L (mV)	$\bar{g}_S$ (nS)	DC (nA)
1	0.34	13.6	−93.1	5.0	0.7/0.8
2	0.39	10.9	−99.0	9.0	0.5/0.9
3	0.33	24.9	−81.7	7.0	0.4/0.6
4	0.412	20.8	−86.0	12.0	0.6/0.9
Cell		g_{e0} (nS)	σ_e (nS)	g_{i0} (nS)	σ_i (nS)
1	LC	6.0	3.0	3.0	1.0
	HC	15.0	5.0	50.0	17.0
2	LC	6.9	3.0	5.1	2.5
	HC	10.1	4.0	25.9	10.0
3	LC	4.0	1.7	3.0	1.5
	HC	7.5	3.0	34.0	15.0
4	LC	5.9	2.9	2.6	1.3
	HC	11.6	5.0	39.4	17.0

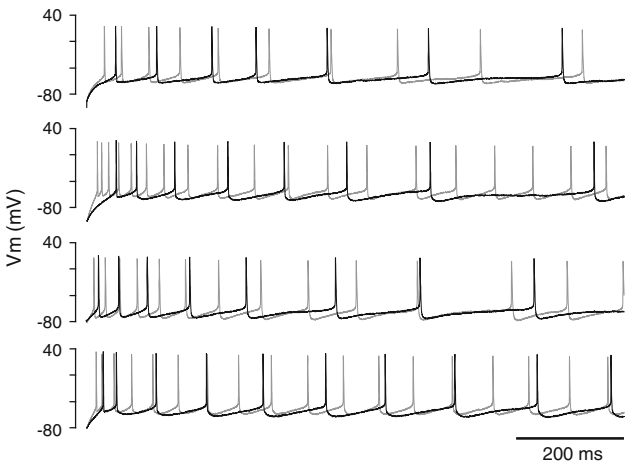

Fig. 1 Response of four cortical pyramidal cells to DC stimulation. *Gray* and *black* traces correspond to two different DC current levels. Parameters are (from top to bottom): cell 1: $C = 0.34$ nF, $g_L = 13.6$ nS, $V_L = -93.1$ mV, DC $= 0.7/0.8$ nA. cell 2: $C = 0.39$ nF, $g_L = 10.9$ nS, $V_L = -99.0$ mV, DC $= 0.5/0.9$ nA. cell 3: $C = 0.33$ nF, $g_L = 24.9$ nS, $V_L = -81.7$ mV, DC $= 0.4/0.6$ nA. cell 4: $C = 0.41$ nF, $g_L = 20.8$ nS, $V_L = -86.0$ mV, DC $= 0.6/0.9$ nA

spontaneous activity was low (up to 6 Hz), for the HC state they were chosen such that they roughly reproduced the mean voltage and its fluctuations during the LC state. For each cell, the PSTH was calculated during either LC or HC states for five different stimulus amplitudes (Figs. 2, 3). In general, during LC states PSTHs are broader and their peaks occur later after stimulus onset than during HC states. Also, the number of spikes per stimulus is higher in the LC state, though the stimulus strength was the same in both states.

Figure 4 compares the performance of all eight models in matching the response to DC stimulation and Fig. 5 shows typical responses of these models. Many models reproduce the experimental data with a good degree of accuracy, while others show a certain deviation.

Surprisingly, the quality of the fit to DC stimulation does not primarily depend on the choice of the adaptation mechanism, but it seems that a nonlinear I–V-curve is a prerequisite for the model to perform well. This naturally includes the HH model, where the nonlinearity stems from the activation of the sodium channel. The flexibility in the HH model is given by a shift in threshold and a scaling of the sodium conductance, whereas during this protocol the shape of the activation curve is kept fixed. However, four models with less parameters than the HH model perform even better, apparently their parametrization is more efficient. Note that the HH model sometimes displays sodium block (as in Fig. 5b; bottom traces), which may explain its moderate performance to fit DC stimulation protocols (but this does not occur for PSTHs—see below).

The best model for this DC stimulation protocol is the adaptive exponential IF model. In this context, it is interesting to note that the pulse-based model, which is a hybrid between the purely linear IF and the HH model, ranks exactly between the two. The Izhikevich model displays the broadest range of fit quality, ranging from one of the best fits of a single cell to the worst fit in the ensemble. However, the fitting of the Izhikevich model turned out to be rather unstable, which is certainly due to the fact that it can change its behavior drastically even for small variations of the parameters. So in this case it is possible that we simply missed the region of parameter space that best corresponds to the data. In conclusion, many different models are able to satisfactorily reproduce the response of cortical neurons to DC stimulation.

The second protocol was intended to reproduce a situation that is close to the conditions encountered by cortical neurons in intact networks during periods of intense activity. Here, we looked at the characteristics of spike initiation on a timescale of a few milliseconds. Figure 6 shows the quality of the fits to the four cells for all eight models. We first fitted the six PSTHs that correspond to the stimulus strengths 1 nS, 2 $\bar{g}_S$, and 4 $\bar{g}_S$ during LC as well as HC states. In all models, spike-related adaptation mechanisms were disabled by setting the appropriate parameters to zero (see Sect. 2). We would like to highlight several points: first, in this protocol the HH model, which is computationally the most costly model, shows the best performance, both for each cell separately (with the exception of the fit of the pulse-based model to cell 4) as well as on average. This might not be too surprising given the large number of parameters that are adjusted. However, the model with the worst performance (again separately for each cell and on average) is the quadratic IF model rather than the linear model one might have expected. Also, again, the Izhikevich model (with spike-related adaptation disabled) shows an unsatisfactory behavior compared to the

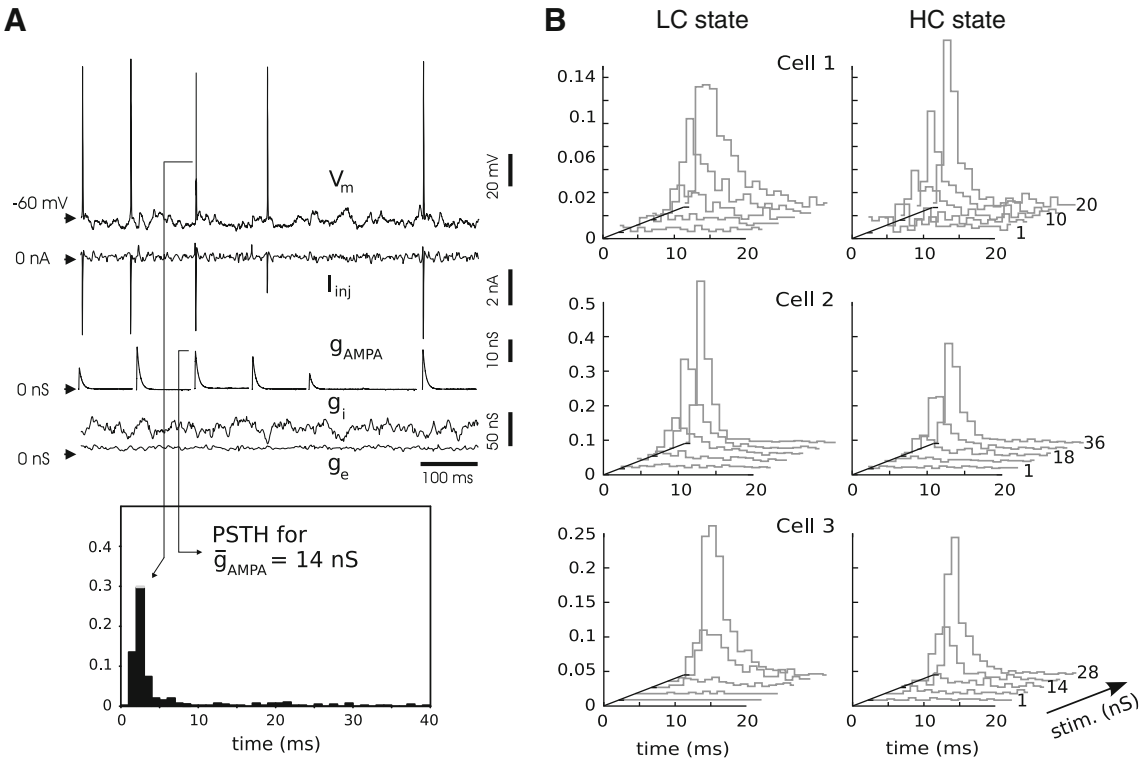

Fig. 2 Experimental protocol and resulting PSTHs. **a** Dynamic-clamp experiment in which two fluctuating conductances (excitatory, g_e and inhibitory, g_i) were injected to recreate in vivo-like background activity. In addition, AMPA-shaped excitatory conductance stimuli (g_{AMPA}) with varying strength were injected into the cell using dynamic clamp. Stimulus amplitudes were randomized, and collected for each stimulus strength separately, to compute PSTHs. **b** Experimental PSTHs calculated for three different cells (a fourth cell is shown in Fig. 3). The x-axis shows time after stimulus onset, the y-axis labels stimulus strength, and the z-axis the probability for generating an action potential (time bin of 1 ms). The *left column* reflects the response during LC states, the right during HC states. Stimulus amplitudes ($\bar{g}_{AMPA}$) were of 1, 5, 10, 15, 20 (cell1); 1, 9, 18, 27, 36 (cell2), and 1, 7, 14, 21, 28 (cell 3) nS

similarly complex adaptive exponential IF model. An explanation for this observation might be the constraints we put on the models, namely to reflect the experimental leak conductance and its reversal potential. This fixes the shape of the quadratic nonlinearity at the leak reversal, but due to its inherent symmetry also to a large extent in the spike initiation region. For the quadratic IF model, the only freedom left is the position of the second root of the parabola. For the Izhikevich model, there are three free parameters left, which slightly betters the quality of its fits. In general, the ranking of cells according to their goodness of fit is similar across models, i.e. cell 4 is usually fit best whereas cell 1 shows the largest deviation. An exception is the linear IF model, most visibly in its fit to cell 3. This cell shows a later onset of spikes following the stimulus, which better suits a quadratic I–V–curve (cf. Fourcaud-Trocmé et al. (2003)). In the absence of noise, the linear IF model can emit spikes only during the rising phase of the EPSP, whereas the nonlinear IF models are able to spike at any time after the stimulus (provided the V_m is sufficiently depolarized, i.e. beyond the second root of the I–V–curve). The presence of synaptic noise tends to blur this effect, but the principal behavior remains.

Finally, the linear-quadratic and the exponential IF as well as the aEIF model and the pulse-based models display a very homogeneous performance in reproducing the experimental PSTHs. The first three combine the advantages of the quadratic IF model (no sharp spike initiation) and the linear IF model (separation of the behavior at rest and at threshold). Apparently, the exact realization of the nonlinearity (quadratic or exponential) is not crucial here. Also, it seems that the presence of an adaptation state variable (with spike-related adaptation disabled) in the aEIF model does not improve the match significantly in this particular context, compared to the 1-state-variable models lqIF and eIF. The pulse-based model on the other hand nicely demonstrates its hybrid character—the smooth spike initiation improves the match with the data, however, it still displays a relative weakness in the fit to cell 3.

We repeated the fit, now allowing all models their own way of spike-related adaptation (see Sect. 2). The results are displayed in Fig. 7. The most apparent difference is clearly

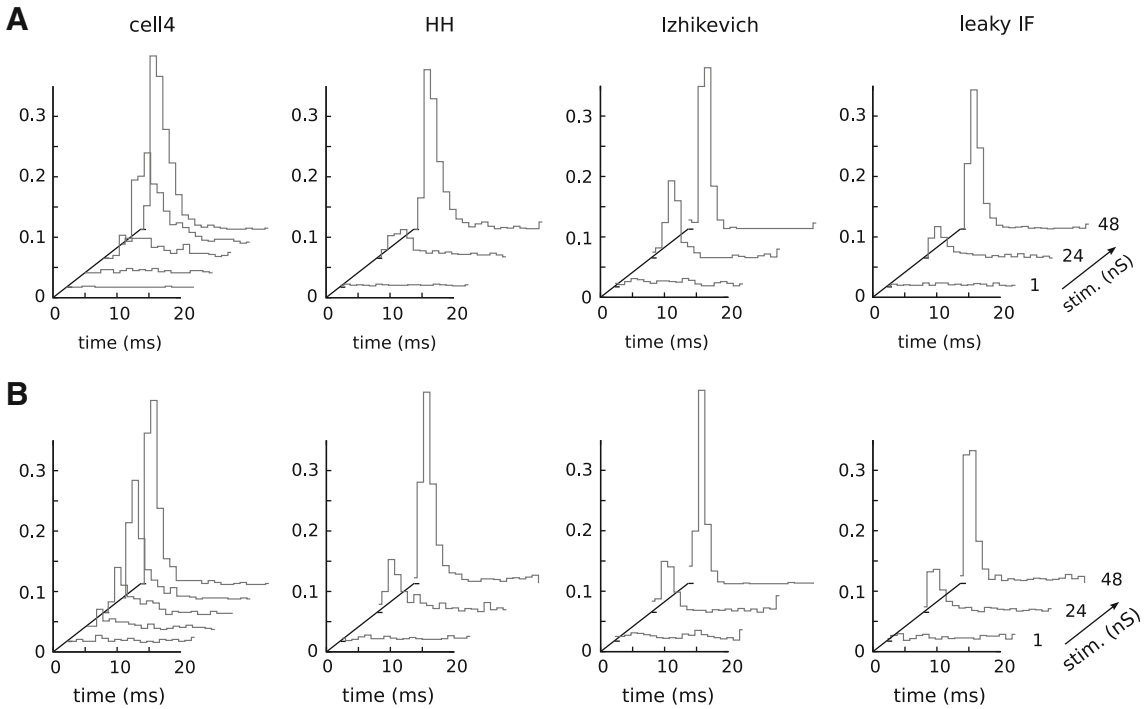

Fig. 3 Comparison between experimental PSTHs and best model fits during LC (A) and HC (B) states simultaneously, adaptation included. *Cell 4:* Experimental PSTHs obtained for cell 4 ($\bar{g}_{\mathrm{AMPA}}$ = 1, 12, 24, 36, 48 nS). *HH* PSTHs of the best-fitted HH model. *Izhikevich* PSTHs of the best-fitted Izhikevich model. *Leaky IF* PSTHs of the best-fitted leaky IF model. For this particular cell, all three models show acceptable to good agreement with the experiments (see error values in Fig. 7)

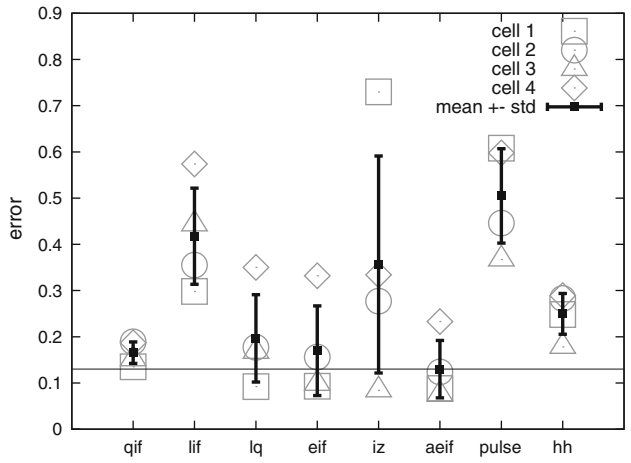

Fig. 4 RMS error for the best fits of all models to all cells during DC stimulation. A nonlinear I–V-curve seems necessary but not sufficient in order to reproduce the experimental traces

the behavior of the Izhikevich model. In agreement with the above results, the fit of cell 3 is the best for this model. However, the strong sensitivity to parameters remains, such that again we were not able to find good fits for all cells. As before, the HH model shows the best match, on an individual level and on average (again with the exception of the fit of the pulse-based model to cell 4). It is followed by the pulse-based model, which again shows a relative weakness for cell 3. On average, the exponential IF model with adaptation performs slightly better than its more elaborate counterpart, the aEIF model. This is not a contradiction: though the definition of both models is very similar, the EIF model with adaptation is not a special case of the aEIF model. While the adaptation mechanism of the first is modeled as a conductance, the adaptation state variable in the aEIF model acts as a current. A relevant comparison can be made between the EIF model without adaptation and the aEIF model with or without spike-related adaptation, and indeed here the EIF always performs worse than its more general counterpart (though not by much). We conclude that, when a spike-related adaptation mechanism is included, most models (except the linear and the quadratic IF models as well as the Izhikevich model) show an acceptable match with the experiments, although each model has its particular strengths and weaknesses depending on the cell.

To determine for each model, which features of the PSTHs were reproduced accurately and which were not, we fitted gamma distributions to both the experimental and the simulated PSTHs. From these fits, we extracted the position and the height of the peaks as well as the "decay time constant" of the falling flanks. In addition we fitted a constant to the PSTH for lowest stimulus strength (which is basically flat) in order to quantify the spontaneous activity. For the data, the spontaneous activity was around 0–6 Hz. Figure 8a shows the RMS

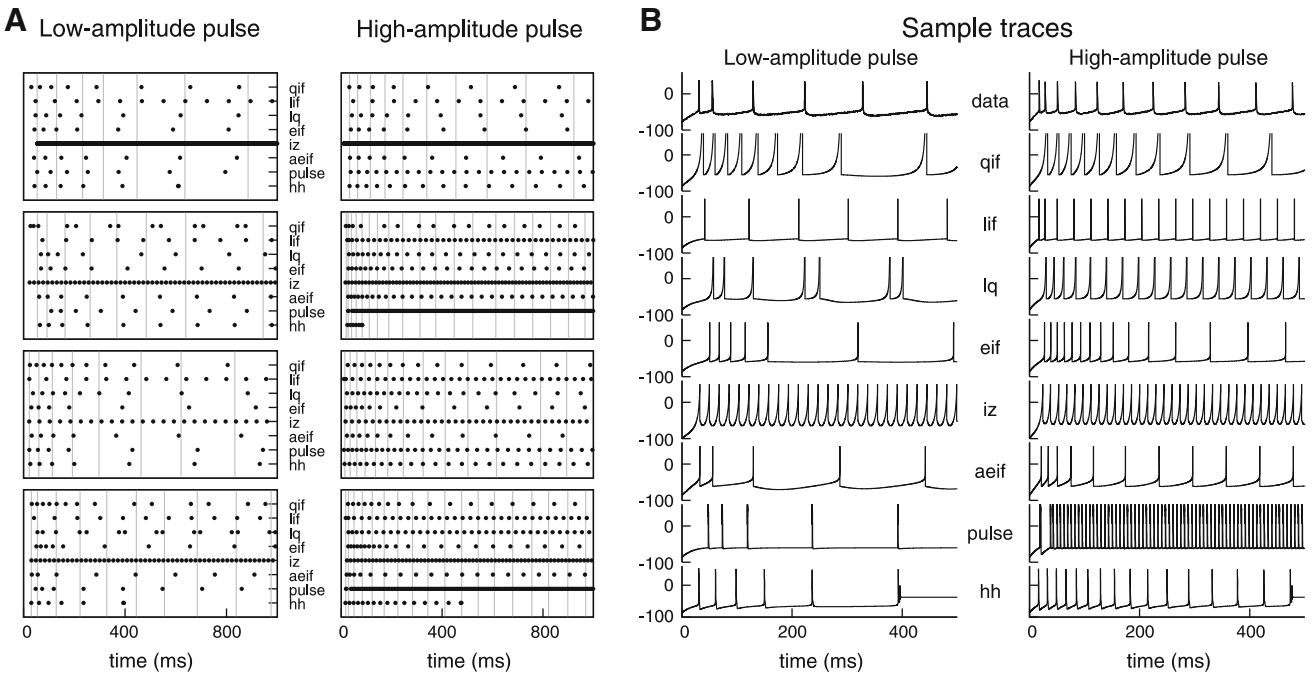

Fig. 5 Raster plots of spike response to DC stimulation of the best fits in the first second after stimulus onset. Stimulus amplitudes were 0.7/0.8, 0.5/0.9, 0.4/0.6, 0.6/0.9 nA (given as low/high stimulus amplitude for cells 1–4). **a** spike times in response to low amplitude (*left panels*) and high-amplitude (*right panel*) stimulation. The *vertical bars* represent the spike times during the experiment, the overlayed *dots* indicate the spikes of the respective fitted models (see label to the right). The four boxes correspond to cells 1–4 (*top* to *bottom*). **b** Sample traces for the data (*top* traces from cell 4) and best fits to DC stimulation (all other traces), with low-amplitude pulses (*left*) and high-amplitude pulses (*right*)

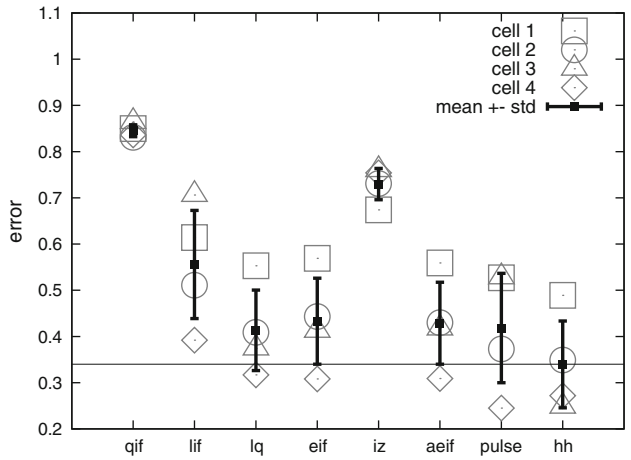

Fig. 6 RMS error for the best fits of all models to all cells without spike-related adaptation during the PSTH protocol. The horizontal line shows the average RMS of the best model (HH). The performance of the leaky IF model strongly depended on the cell, the match of the quadratic IF and the Izhikevich model with experiment was generally unsatisfactory. All other models showed good performance

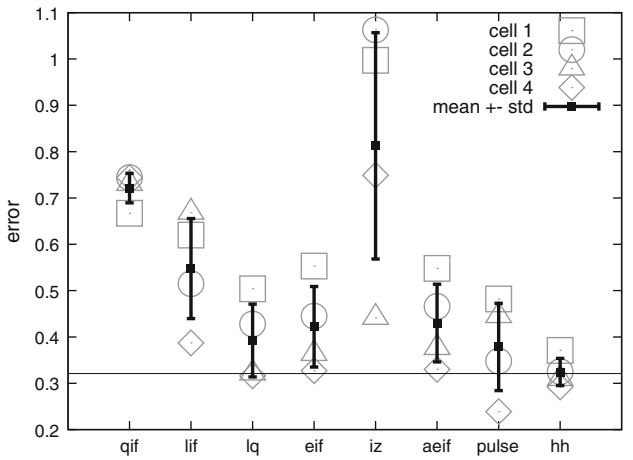

Fig. 7 RMS error for the best fits of all models to all cells with spike-related adaptation. The *horizontal line* shows the average RMS of the best model (HH). In general, the fits were better compared to Fig. 6

of the difference in spontaneous activity with respect to the different models. The difference is smallest for the linear IF and the Izhikevich model. However, the contribution of this feature to the error function is minor, so one cannot really expect a good match between the simulation of these models and experiment. The three remaining panels show an indication of which aspects of the PSTHs account for the high errors seen for the linear and the quadratic IF models. The qIF performs particularly badly in terms of the location of

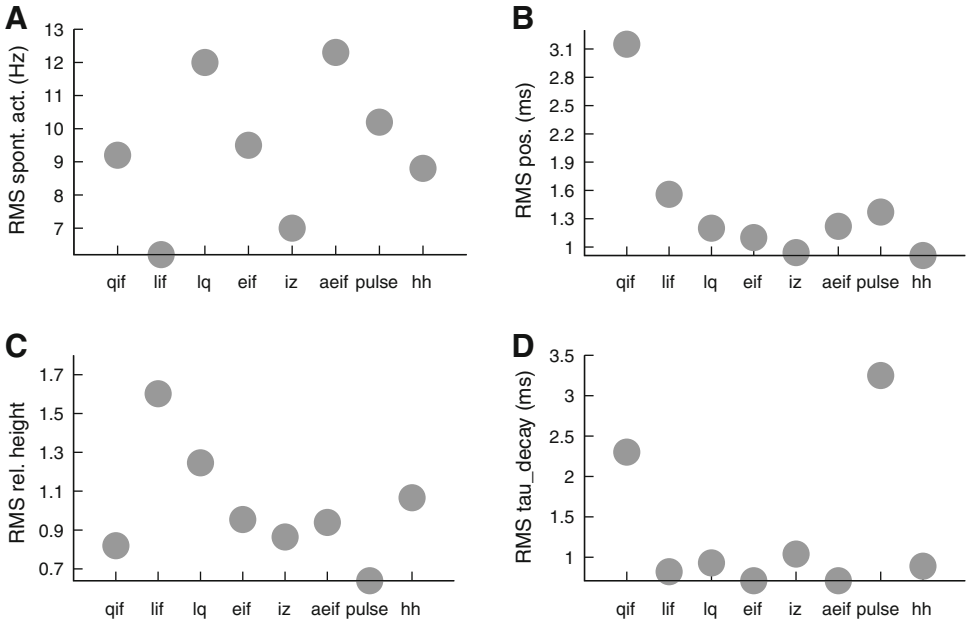

Fig. 8 Comparison of different characteristics of the PSTHs. The RMS error of the difference between the experimental and the model PSTHs are given. **a** spontaneous activity. **b** PSTH peak position. **c** relative peak height. **d** PSTH decay time constant

the PSTH peak (Fig. 8b), as well as the decay time constant of the PSTH flanks (Fig. 8d), indicating inaccurate timing of the response. In contrast, the leaky IF model performs well by these 2 measures, but displays a high error in the PSTH height (Fig. 8c), indicating a well-timed response of inaccurate amplitude (see also the examples in Fig. 4). The remaining models display a combination of features that are not easily related to the error values. The IZ model does not display one prominent source of error. The HH model is good at reproducing PSTH peak position and decay time constants (response timing) but less so the PSTH height (amplitude), while the pulse model is poor in terms of decay time constant but excellent in terms of PSTH height (amplitude): both these models perform well according to Fig. 7. These results indicate that the error function used is sensitive to both the timing and amplitude aspects of the response, and a model's relative weakness in one aspect can sometimes be compensated by its strength in the other aspect. Finally, we tested whether fitting the model response to the LC and HC background at the same time added constraints, or if a fit using each background separately would have yielded similar results. To this end, we first ran a fit (adaptation included) of the PSTHs obtained during either LC or HC background (using the same sequence of stimulus strengths as before). With the model parameters obtained in this manner, we subsequently ran simulations using the respective other background state and computed the PSTHs. We termed the PSTHs obtained during a LC state, but using the parameters corresponding to a fit in the HC state, the "LC prediction" and vice versa. Figure 9 summarizes the results: the lower end of each vertical bar indicates the minimal error obtained during a fit during either LC (top) or HC (bottom) state, the upper end

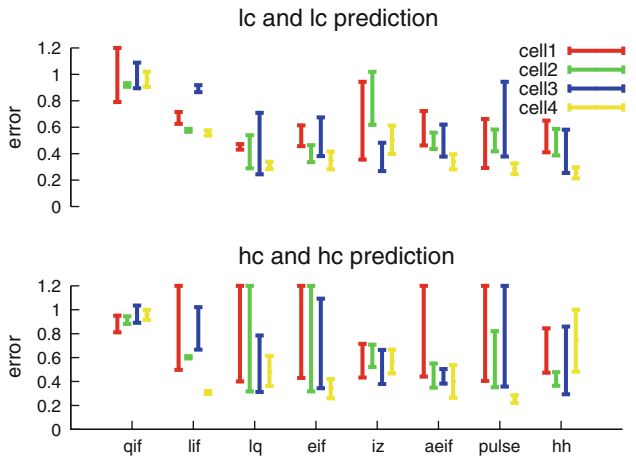

Fig. 9 Quality of model predictions of data not used in the fitting. *Top* all models were fit to PSTHs only for the LC state, and the optimal fits to the HC state were used to predict the responses during the LC state. Each bar joins the RMS error of the fit (lower end of the bar) to the RMS error of the prediction (higher end of the bar). Different *colors* correspond to different cells, as shown in the *inset*. *Bottom* same approach, but models are fit to the HC response and are compared to the HC prediction using the parameters obtained from the fit during the LC state

represents the error of the respective prediction. The length of the bar thus represents the discrepancy between the best fit and the prediction. With only a few exceptions, all fits to a single background state have lower error values than the fits to both states at the same time (not shown).[1] The mismatch

[1] Note that the exceptions are justified, since only the "mean" (roughly speaking) should be lower or equal to the error from the fit to both states

between a PSTH and its respective prediction does not seem to be related to a specific model or cell.

In general, the parameters obtained during the fit to one background state do not reproduce well the behavior during the respective other.

4 Discussion

In this article, we have presented a comparison of the ability of eight neuron models to reproduce in vitro recordings in a quantitative way. The main originality of the data set is (1) that we have used a whole series of PSTH computed in pyramidal neurons for different input intensities, in addition to classic DC current injection; (2) all PSTHs were obtained with conductance-based inputs in dynamic-clamp experiments; (3) PSTHs were obtained in two different conditions of background activity and conductance state of the membrane. The latter constitutes a strong constraint because the amplitude and kinetics of the PSTHs obviously depend on the conductance state.

The originality in terms of modeling is that we considered a large range of different models, ranging from very simple models, such as the IF model and its quadratic, exponential or pulse-based variants, two-variable IF models of intermediate complexity, and the more complex HH-type models. These models are characterized by different complexity in terms of the number of variables and the number of parameters to be adjusted.

Fitting these different models to the responses to DC stimulation alone revealed that the quality of the fit did not crucially depend on model complexity, but a condition for a good reproduction seemed to be a nonlinear I–V-curve. This condition is not sufficient, however, as illustrated by the overall bad performance of the Izhikevich model.

The conclusion was very different when considering the more extended data set consisting of families of PSTHs in response to conductance-based excitatory inputs, in two different conductance states. This analysis revealed that the presence of spike-related adaptation improved the match between experiments and simulations, which is expected because RS cells display prominent spike-frequency adaptation. Additional model complexity yielded a better match with experiments in general. However, the surplus in accuracy can be very costly computationally. This observation was valid for the fits to either LC or HC state separately, or to both at the same time. The HH model, for example, performed best of all models overall, with and without adaptation included. However, the simpler nonlinear IF models (with the exception of the quadratic IF model) and the pulse-based model came surprisingly close. We conclude that these models constitute very good candidates for simulations of networks of RS neurons if computational efficiency needs to be optimized.

We also found that the best fit for a model does depend on the state (LC or HC) that the neuron is in. Fitting the response to stimuli during one state at a time usually entailed a bad match during the respective other state. In Herrmann and Gerstner 2001, 2002, an analytical derivation of the PSTH shape has been given during conditions that are comparable though not exactly the same as here. The authors used current-based inputs and an escape noise model. One of their results is the description of the PSTH shape as a superposition of the stimulus waveform and its first derivative, the relative importance of the two depending on the level of noise. Given the low level of spontaneous activity in our recordings, the comparison with their results is difficult. However, conforming with their results and our choice of noise parameters ($0.3 \leq \sigma/g_0 \leq 0.5$), the absence of secondary peaks and a strong trough after the main peak indicates that our recordings were done in a high-noise regime.

A crucial point in fitting experimental data with computational models is always the choice of the error function (Van Geit et al. 2008), and our choice is by far not the only one possible. Another possibility would have been to allow an equal importance of all stimulus strengths by scaling the corresponding partial error. This would have given more importance to the lower stimulus amplitudes than is realized here, thus emphasizing spontaneous activity. Alternatively, a "multiple objective optimization approach" (Druckmann et al. 2007) could have been used on the features extracted from the fit, where a new set of parameters is only assumed to be superior when it results in an ensemble of features that all fit the data better than the previous best set of parameters.

Finally, it must be stressed that the particular protocols that we have chosen here are just two possibilities among many others in order to characterize neuronal behavior. Another very relevant approach is the exact reproduction of spike times in response to noisy stimuli (Jolivet et al. 2006; Jolivet et al. 2008; Clopath et al. 2007). Such an approach was not attempted here, as we used error functions in which the timing of individual spikes is not taken into account. In our case, since we are interested in the neuron's response to additional (e.g., sensory) inputs in the context of ongoing synaptic noise, it does not make sense to compare individual spike times. We instead turned to the PSTH as a statistical characterization of the neuron's response (another alternative would be to use the probability to spike in response to a given input, as was done in Destexhe et al. 2003, or Wolfart et al. 2005; however, information about spike timing would then be lost). In our approach, the fluctuating background is a source of noise,

Footnote 1 continued
at the same time. This explains why a fit using less constraints (only LC or HC) can be worse than fits that used the whole data set (LC and HC).

while in the approach of the Gerstner's group, the fluctuating inputs constitute the signal itself. Only future studies of in vivo neuronal processing will tell which approach is better suited for which type of activity in the nervous system.

Previous studies also have compared different types of models, including HH models (Kobayashi et al. 2009). Note that we had a particularly difficult time to optimize the HH model because of the large number of parameters (ten parameters in our case). This may explain the surprisingly bad performance of the HH model in that study (see Kobayashi et al. 2009). Alternatively, sodium block may occur for the HH model (as seen in Fig. 5b), and could also artificially diminish its global fitting performance. This emphasizes that the choice of an appropriate search method is critical in the interpretation of such results. Other approaches, such as direct fitting of the I–V-curve (Badel et al. 2008) do not suffer from such problems, but this latter method is only applicable to a given class of models (it cannot be used for HH models for instance).

Future work should consider not only responses to isolated excitatory inputs, but complex responses to streams of several excitatory and inhibitory inputs. This approach should provide much more severe constraints on models and is also closer to the situation of input integration in real networks. However, for such complex stimuli, there is a combinatorial explosion of the number of possible configurations, and realizing them experimentally would necessitate several hours of stable recording, which certainly constitutes the most challenging aspect of this type of experiment.

Acknowledgments We thank Andrew Davison for the NEURON implementation of the fitting algorithm. Research supported by the CNRS, the ANR (HR-Cortex, Complex-V1) and the European Community (FACETS project FP6 15879), and cluster computing time was provided thanks to the *Neuroinformatics* program of the CNRS.

References

Achard P, De Schutter E (2006) Parameter landscape for a complex neuron model. PLoS Comput Biol 2:794–804

Badel L, Lefort S, Brette R, Petersen CH, Gerstner W, Richardson MJE (2008) I–V curves are reliable predictors of naturalistic pyramidal-neuron voltage traces. J Neurophysiol 99:656–666

Brette R, Gerstner W (2005) exponential integrate-and-fire model as an effective description of neuronal activity.. J Neurophysiol 94:3637–3642

Brette R, Piwkowska Z, Monier C, Rudolph-Lilith M, Fournier J, Levy M, Frégnac Y, Bal T, Destexhe A (2008) intracellular recordings using a real-time computational model of the electrode.. Neuron 59:379–391

Clopath C, Jolivet R, Rauch A, Lüscher HR, Gerstner W (2007) Predicting neuronal activity with simple models of the threshold type: Adaptive Exponential Integrate-and-Fire model with two compartments.. Neurocomputing 70:1668–1673

Destexhe A (1997) Conductance-based integrate-and-fire models. Neural Comput 9:503–514

Destexhe A, Mainen ZF, Sejnowski TJ (1994) An efficient method for computing synaptic conductances based on a kinetic model of receptor binding. Neural Comput 6:14–18

Destexhe A, Rudolph M, Fellous JM, Sejnowski TJ (2001) Fluctuating synaptic conductances recreate in-vivo-like activity in neocortical neurons. Neuroscience 107:13–24

Destexhe A, Rudolph M, Paré D (2003) The high-conductance state of neocortical neurons in vivo. Nat Rev Neurosci 4:739–751

Druckmann S, Banitt Y, Gidon A, Schürmann F, Markram H, Segev I (2007) A novel multiple objective optimization framework for constraining conductance-based neuron models by experimental data. Frontiers Neurosci 1:7–18

Ermentrout GB (1996) Type 1 membranes, phase resetting curves, and synchrony. Neural Comput 8:979–1001

Fitzhugh R (1961) Impulses and physiological states in models of nerve membrane. Biophys J 1:445–466

Fourcaud-Trocmé N, Hansel D, van Vreeswijk C, Brunel N (2003) How spike generation mechanisms determine the neuronal response to fluctuating inputs. J Neurosci 23:11628–11640

Goaillard JM, Taylor AL, Schulz DJ, Marder E (2009) Functional consequences of animal-to-animal variation in circuit parameters. Nature Neurosci 12:1424–1430

Herrmann A, Gerstner W (2001) Noise and the PSTH response to current transients: I. General theory and application to the integrate-and-fire neuron. J Comput Neurosci 11:135–151

Herrmann A, Gerstner W (2002) Noise and the PSTH response to current transients: II. Integrate-and-fire model with slow recovery and application to motoneuron data. J Comput Neurosci 12:83–95

Hines ML, Carnevale NT (1997) The NEURON simulation environment. Neural Comput 9:1179–1209

Hodgkin AL, Huxley AF (1952) A quantitative description of membrane current and its application to conduction and excitation in nerve. J Physiol 117:500–544

Izhikevich EM (2003) Simple model of spiking neurons. IEEE Trans Neural Networks 14:1569–1572

Izhikevich EM (2004) Which model to use for cortical spiking neurons?. IEEE Trans Neural Networks 15:1063–1070

Jolivet R, Lewis TJ, Gerstner W (2004) Generalized integrate-and-fire models of neuronal activity approximate spike trains of a detailed model to a high degree of accuracy. J Neurophysiol 92:959–976

Jolivet R, Rauch A, Lüscher HR, Gerstner W (2006) Predicting spike timing of neocortical pyramidal neurons by simple threshold models. J Comput Neurosci 21:35–49

Jolivet R, Schürmann F, Berger TK, Naud R, Gerstner W, Roth A (2008) The quantitative single-neuron modeling competition. Biol Cybern 99:417–426

Kobayashi R, Tsubo Y, Shinomoto S (2009) Made-to-order spiking neuron model equipped with a multi-timescale adaptive threshold. Frontiers Comput Neurosci 3:9

Lapicque L (1907) Recherches quantitatives sur l'excitation electrique des nerfs traitée comme une polarisation. J Physiol Pathol Gen 9:620–635

Latham PE, Richmond BJ, Nelson PG, Nirenberg S (2000) Intrinsic dynamics in neuronal networks. I. Theory. J Neurophysiol 83:808–827

Le Franc Y, Foutry B, Nagy F, Le Masson G. (2001) Nociceptive signal transfer through the dorsal horn network: hybrid and dynamic clamp approaches using a real-time implementation of the Neuron simulation environment. Soc Neurosci Abstracts 27: 927.18

Le Masson G, Maex R. Introduction to equation solving and parameter fitting. In: De Schutter E, editor. Computational neuroscience: realistic modeling for experimentalists. CRC Press, London

Morris C, Lecar H (1981) Voltage oscillations in the barnacle giant muscle fiber. Biophys J 35:193–213

Nagumo JS, Arimoto S, Yoshizawa S (1962) An active pulse transmission line simulating nerve axon. Proc IRE 50:2061–2070

Piwkowska Z, Pospischil M, Brette R, Sliwa J, Rudolph-Lilith M, Bal T, Destexhe A (2008) Characterizing synaptic conductance fluctuations in cortical neurons and their influence on spike generation. J Neurosci Methods 169:302–322

Pospischil M, Toledo-Rodriguez M, Monier C, Piwkowska Z, Bal T, Frégnac Y, Markram H, Destexhe A (2008) Minimal Hodgkin-Huxley type models for different classes of cortical and thalamic neurons. Biol Cybern 99:427–441

Press WH, Flannery BP, Teukolsky SA (1992) Numerical Recipes in C: The Art of Scientific Computing, 2nd edn. Cambridge University Press, Cambridge

Robinson HP, Kawai N (1993) Injection of digitally synthesized synaptic conductance transients to measure the integrative properties of neurons. J Neurosci Methods 49:157–165

Sadoc G, Le Masson G, Foutry B, Le Franc Y, Piwkowska Z, Destexhe A, Bal T (2009) Recreating *in vivo*–like activity and investigating the signal transfer capabilities of neurons: dynamic-clamp applications using real-time NEURON. In: Destexhe A, Bal T (eds) Dynamic-clamp: from principles to applications. Springer, New York

Sharp AA, O'Neil MB, Abbott LF, Marder E (1993) Dynamic-clamp: computer-generated conductances in real neurons. J Neurophysiol 69:992–995

Traub RD, Miles R (1991) Neuronal networks of the hippocampus. Cambridge University Press, Cambridge

Van Geit W, De Schutter E, Achard P (2008) Automated neuron model optimization techniques: a review. Biol Cybern 99:241–251

Vanier MC, Bower JM (1999) A comparative survey of automated parameter-search methods for compartmental neural models. J Computational Neurosci 7:149–171

Weaver CM, Wearne SL (2006) The role of action potential shape and parameter constraints in optimization of compartment models. Neurocomputing 69:1053–1057

Wolfart J, Debay D, Le Masson G, Destexhe A, Bal T (2005) Synaptic background activity controls spike transfer from thalamus to cortex. Nature Neurosci 8:1760–1767

Yamada WM, Koch C, Adams PR (1989) Multiple channels and calcium dynamics. In: Koch C, Segev I (eds) Methods in neuronal modeling. MIT press, Cambridge